Journal of Physics D: Applied Physics

Electrical characteristics of interfacial barriers at metal—TiO_2 contacts

OPEN ACCESS
IOP Publishing
Journal of Physics D: Applied Physics
J. Phys. D: Appl. Phys. **51** (2018) 425101 (13pp)
https://doi.org/10.1088/1361-6463/aadbd2

Electrical characteristics of interfacial barriers at metal—TiO_2 contacts

L Michalas[1], A Khiat, S Stathopoulos and T Prodromakis

Electronic Materials and Devices Research Group, Zepler Institute for Photonics and Nanoelectronics, University of Southampton, Southampton, SO17 1BJ, United Kingdom

E-mail: l.michalas@soton.ac.uk

Received 15 June 2018, revised 14 August 2018
Accepted for publication 20 August 2018
Published 10 September 2018

Abstract

The electrical properties of thin TiO_2 films have recently been extensively exploited with the aim of enabling a variety of metal-oxide electron devices: unipolar and bipolar semiconductor devices and/or memristors. In these efforts, investigations into the role of TiO_2 as active material were the main focus; however, electrode materials are equally important. In this work we address this point by presenting a systematic quantitative electrical characterization study on the interface characteristics of metal-TiO_2-metal structures. Our study employs typical contact materials that are used both as top and bottom electrodes in a metal-TiO_2-metal setting. This allows an investigation of the characteristics of the interfaces as well as holistically studying an electrode's influence on the opposite interface, referred to in this work as the top/bottom electrodes inter-relationship. Our methodology comprises the recording of current–voltage (I–V) characteristics from a variety of solid-state prototypes in the temperature range of 300 K –350 K, and their analysis through appropriate modelling. Clear field- and temperature-dependent signature plots were also obtained, so as to shine more light on the role of each material as top/bottom electrodes in metal-TiO_2-metal configurations. Our results highlight that these are not conventional metal–semiconductor contacts, and that several parameters are involved in the formation of the interfacial barriers, such as the electrode's position (atop or below the film), the electronegativity, the interface states, and even the opposite interface electrode material. Overall, our study provides a useful database for selecting appropriate electrode materials in TiO_2-based devices, offering new insights into the role of electrodes in metal-oxide electronics applications.

Keywords: TiO_2, metal electrodes, Schottky barrier, RRAM, TFT, selectors

(Some figures may appear in colour only in the online journal)

1. Introduction

Metal oxides (MOs) have a unique ensemble of properties with great potential to meet the diverse requirements of modern electronics. Specifically, they offer low temperature (<100 °C) manufacturability [1] and thus compliance with large-scale uniformity and deployment on alternative materials (paper, flexible); adequate device level mobility [2] that can be further optimised by engineering appropriate gate dielectrics; high transparency due to their wide band gap; the capacity for post-fabrication tunable resistance (memristive effects) [3, 4], and good chemical stability. These features have led to the use of MOs in a variety of applications ranging from resistive random access memories (RRAMs) [5, 6] and thin film transistors (TFTs) [7, 8] to oxide-based photovoltaics [9] and sensors [10], introducing a new era for large area transparent/stretchable electronics [11, 12] and neuromorphic systems [13, 14]. It is also worth mentioning two very recently published perspective articles [15, 16] discussing this envisioned new era. To this end, a variety of materials have

[1] Author to whom any correspondence should be addressed.

been scrutinised over recent years with distinct MOs (and thus properties) being exploited according to the requirements of the application, e.g. neuromorphic applications favour MO devices that show a large memory capacity [4].

TiO_2 is without a doubt one of the most celebrated materials through practical implementations of memristors [17], TFTs [18, 19], sensors [20], and corollary applications of these. The ability of TiO_2 to obtain varying microstructures (i.e. amorphous, micro- and nano-crystalline, rutile, anatase, etc), and thus a plethora of electronic properties that can be determined or controlled by the fabrication and/or biasing conditions, has augmented its use in practical applications. This is further enhanced by the incorporation of foreign metal elements (doping) in TiO_2 thin films, which was shown to improve RRAM switching characteristics [21] and also to enable both n- and p-type functionalities [22, 23]. The latter area is still in its infancy, but offers substantial prospects for low-temperature manufacturable electronic systems. Research efforts are thus targeted at addressing outstanding challenges [24], with first proof-of-concept results on the development of bipolar components based entirely on TiO_2 p-n homo-junctions [25, 26] showcasing the exciting technological potential.

Notwithstanding the importance of the oxide active layer, identifying appropriate metal contacts and deciphering their interfacial role is now of paramount importance to a device's electrical behaviour. This role becomes even more important in highly scalable thin-film structures where their properties strongly rely on interfacial effects. Considering the up-to-date studies, metal contacts on oxide materials appear to be attracting important and continuously increasing research attention. Various metals on various oxide materials have been assessed, and focused methods have been introduced aiming at both the development of reliable contacts [27] and an understanding of the formation mechanism [28, 29]. Moreover, important advances in understanding the nature of metal/oxide (electrolyte) contacts are also being made in the field of RRAM cells, revealing the interesting nano-battery effect [30] and highlighting the role redox processes [31] of interfacial layers [32] and moisture [33]. These aspects were recently summarized in a topical review [34]. All the above suggest that these are not conventional metal–semiconductor contacts where the metal work function dominates the process. Fabrication details [27, 35], environmental conditions [36] and electrochemical interactions [37] all make significant contributions as well.

More specifically, regarding the metal-TiO_2 contacts, it was reported that recording the rectification ratio measured at a read-out voltage of ± 1 V for a variety of top electrodes (TEs) (deposited by RF magnetron sputtering on a metal-TiO_2-(non-rectifying-Pt) configuration) can reveal the role of a metal's electronegativity on the formation of the interface barrier [38]. In the same study, barriers evaluated by the forward diode current suggested partial Fermi level pinning. In addition, the role of the TE (evaporated through a shadow mask) on a metal-TiO_2-(non-rectifying-Pt) memory cell, evaluated with a read-out voltage of ± 1 V, was correlated to the formation free energy for the top metal electrode oxide [39]. Moreover, the symmetry or asymmetry of metal-TiO_2-(non-rectifying-Al) current–voltage characteristics was also attributed to the top metal fabrication details, such as the thermal annealing [40]. More recently, the source and drain electrodes of TiO_2-based TFTs were found to play a major role on performance parameters such as the on/off ratio and the field effect mobility [19]. All the above assessments are restricted to room temperature semi-quantitative approaches, focusing only on studying electrodes formed on top of TiO_2 films.

In this paper we present a detailed quantitative electrical characterization study of metal-TiO_2 interface characteristics. The work involves the commonly used contact metals acting as both top and bottom contacts in metal-TiO_2-metal configuration; it also reports the influence of the TE material on the bottom electrode (BE) interface. This is performed by recording the current–voltage (I–V) characteristics at different temperatures and through appropriate modelling and analysis that includes field- and temperature-dependent signature plots. Considering also the potential applications, the design and fabrication of all prototyped samples on which this study was based remained aligned to standard low-temperature microelectronic processes, while the electrodes were patterned through optical lithography and deposited via electron-beam evaporation.

2. Experimental

The tested devices were fabricated on two separate six-inch Si wafers having a 200 nm thick SiO_2 layer that was grown by dry oxidation at 1000 °C with 5 slm of O_2 flow. All electrodes and active areas were patterned via standard optical lithography and lift-off processes [41]. The first fabricated wafer was prepared in order to study the influence of TE metal variations on the performances of devices. Therefore, a common BE metal was used, Au, with a thickness of 20 nm preceded by a 5 nm Ti adhesive layer. The TiO_{2-x} core film was deposited on top of the Au BE by Lambda-controlled plasma-assisted reactive magnetron sputtering (Helios Pro XL, Leybold Optics) using a Ti target, with 8 sccm O_2, 35 sccm Ar flows and 2 kW at the cathode, and 15 sccm O_2 flow and 2 kW at an additional plasma source. This industrial tool provides high-quality films with low thickness variations across the wafer. Using a Woolham MD2000D ellipsometer, the TiO_{2-x} thickness across a six-inch wafer was found to be 24.09 ± 0.16 nm (see the ellipsometry measurements shown in figure 1(c)).

Films deposited by the above procedure exhibit an amorphous and almost stoichiometric nature of TiO_{2-x}, with x in the range of 0.05–0.10, as previously demonstrated in the x-ray absorption spectroscopy study [42]. For the TEs, five separate areas were defined for the depositing of different TE metals: Al, Ti, Ni, Pt and Au, with thicknesses of 15 nm deposited by electron beam evaporation at a low rate of 0.5 Å s^{-1}, for better uniformity, and comparable to deposition rate of the BE.

A similar fabrication flow was adopted for the fabrication of the second wafer, which was dedicated to a study of the influence of the BE metal variations on the performances of TiO_2-based (24 nm) devices. In this wafer, four BE metals

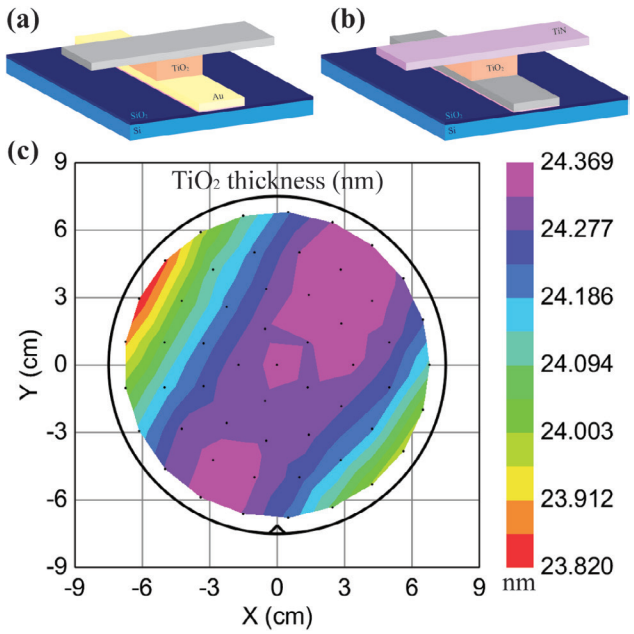

Figure 1. Two wafers were fabricated. The first (a) was dedicated to the study of different TE materials (Al, Ti, Ni, Au, and Pt, shown in grey in (a)), having a common Au BE. The second wafer (b) was dedicated to the study of different BEs with an identical TiN TE (Au, Ti, Ni, and Pt, shown in grey in (b)). In both cases, highly uniform (24.09 ± 0.16 nm) amorphous TiO_{2-x} films (c) were deposited as active area.

were chosen; Ti, Ni, Pt and Au, with thicknesses of 15 nm. A 5 nm Ti layer was also used, for adhesive purposes. After TiO_2 active film deposition and patterning, the same metal (15 nm TiN) was sputtered across the wafer, serving as the TE for all four combinations.

The current versus voltage (I–V) characteristics were obtained on 30×30 μm^2 devices using our in-house memristor characterization platform ArC ONE™ [43]. The voltage sweeping was carried out in staircase mode towards positive biases, while both positive and negative polarities were always applied to the TE with respect to the BE that was continuously kept grounded. All experiments were performed on a Cascade Summit 12000B semi-automatic probe station that incorporates a thermal chuck, the temperature of which can be controlled by an Espec ETC-200L unit. Measurements were performed in the temperature range of 300 K–350 K. The discontinuity appearing at $V = 0$ V in some I–V curves is a result of our data acquisition system that does not acquire this point. The effect is negligible in most of the cases, but not when measuring more conductive samples and for higher temperatures (340 K–350 K), when the conductivity/current further increases. However, this has no effect on the measured data. Finally, it is worth mentioning the role of moisture, which was reported to affect both the transport and switching properties [36, 37, 44] of devices based on sputtered oxide films due to their porous structure. Despite this effect having not shown significant influence in the case of TiO_2 layers [44], our experimental procedure was performed in an environment where humidity and temperature were carefully controlled in order to minimize their influence on the measurements.

3. Results and discussion

3.1. Device modelling and parameters extraction

The studied metal-TiO_2-metal devices are presented in figure 2(a). In order to obtain quantitative results the tested devices were modelled by the equivalent circuit presented in figure 2(b). This consists of two series resistances accounting for the top (R_{TE}) and the bottom (R_{BE}) access electrodes and the device under test (DUT). As TiO_2 exhibits an intrinsic n-type character [23], the DUT can be considered as two inverse polarised Schottky diodes, both emulating the TE and BE contacts, connected through a resistance that corresponds to the TiO_2 core. This equivalent circuit was further used for calculating the effective applied bias (V_{eff})/electric field across the DUT, with respect to the bias applied through the voltage source (V_S) and as a function of the measured current (I), summarised by equation (1):

$$V_{eff} = V_S - I\left(R_{TE} + R_{BE}\right). \tag{1}$$

In the absence of an interface barrier, the Schottky diodes (TE and BE) can be considered as short-circuit. In this case the I–V characteristic should be symmetric with respect to the applied bias polarity and the dominant transport mechanism is determined purely by the properties of the active layer film. For the wide band gap materials, various mechanisms may dominate the transport. Most of them are critically affected by the density and the energy distribution of the band gap states, and spatially by the film microstructure, e.g. conduction paths across the grain boundaries commonly exist in nanocrystalline films [45]. Depending on the applied electric field intensity and the operation temperature, transport may be dominated by hopping, space charge limited currents, the Frenkel–Poole effect, or even by free carriers in the bands [46]. The contribution of internal point defect-related ionic motions [47, 48] and/or those originating from the electrodes should also be taken into consideration. In particular for TiO_2 films, the Ti/TiO_2/Ti stack appears to be very useful for these studies as it allowed for a detailed assessment of the core material controlled conduction mechanism [49, 50]. The latter is supported by our results, as Ti was found to form ohmic or non-rectifying contact when used both as a TE and as a BE.

Interface-controlled transport is typically identified by an asymmetric I–V characteristic with respect to the applied bias polarity. The transport is then dominated by either tunnelling through the barrier formed at the interface or by thermionic emission over it. The two mechanisms can be distinguished via the temperature dependence of the I–V [46].

Tunnelling currents obey the following equation (2):

$$I \propto V^2 \exp\left(-\frac{b}{V}\right) \tag{2}$$

with b being just a constant. Consequently, an asymmetric, temperature-independent I–V supporting also a linear relation on a $\ln(I/V_{eff}^2)$ versus $1/V_{eff}$ signature plot serves as a strong indication of tunneling-dominated transport.

Conversely, thermionic emission over the interface barrier is the most common thermally-activated mechanism

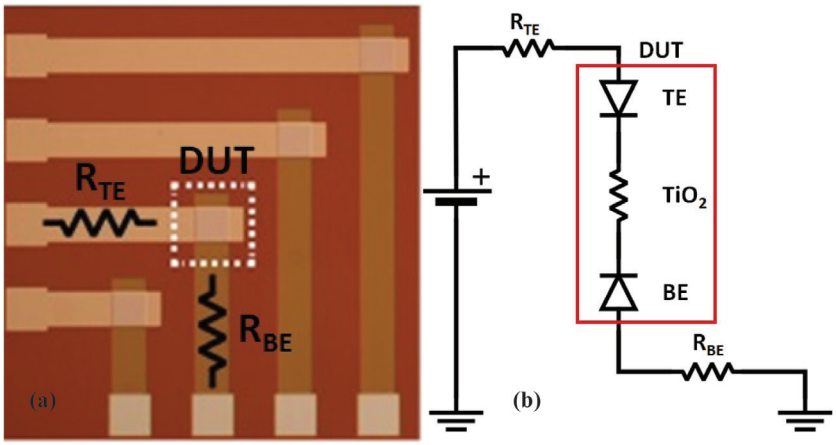

Figure 2. The studied metal-TiO_2-metal devices (a). The equivalent circuit was used to model the devices and the electrodes for our quantitative analysis.

for interface-controlled transport. For those Schottky-type contacts the current flow depends on whether the contact is forward or reverse biased. The forward current–voltage characteristic is given by equation (3):

$$I_{for} = AT^2 \exp\left(-\frac{q\Phi_{B0}}{KT}\right)\left\{\exp\left(-\frac{q\,(V - I_{for}R)}{nKT}\right) - 1\right\} \tag{3}$$

while the reverse biased case can be described by equation (4):

$$I_{rev} = AT^2 \exp\left(-\frac{q(\Phi_{B0} - a\sqrt{V})}{KT}\right) \tag{4}$$

where K is the Boltzmann constant, T is the absolute temperature, Φ_{B0} is the zero bias potential barrier height at the metal/MO interface, $A = (\text{area} \times A^*)$, with A^* being the Richardson constant, n is the ideality factor, 'α' is the barrier lowering factor, q is the electron charge, and R stands for any series resistance.

For the cases where an interface barrier is formed, which is the main focus of this work, any positive bias applied to the TE will result in a forward biased TE/TiO_2 contact and reverse biased TiO_2/BE contact. This is the system of two back-to-back Schottky contacts that is described in detail in [51]. In our case, we emphasize our analysis in the regime where the current flow is determined by the reverse biased BE, given that this constitutes the most resistive element in this series configuration, and thus as a first approximation we may assume that $V_{eff} \approx$ V. The situation is the opposite when a negative bias is applied to the TE; then the TE will determine the current flow.

For this regime, a straight line on a $\ln(I/T^2)$ versus $1000/T$ plot for any applied electric field serves as strong evidence of thermionic emission. The slope of this line corresponds to the apparent interface barrier (Φ_{App}) and should decrease by increasing the applied electric field/bias, as:

$$\Phi_{App} = \Phi_{B0} - \alpha\sqrt{V_{eff}}. \tag{5}$$

If this Φ_{App} versus $V_{eff}^{1/2}$ signature plot is also supported by the extracted results, then the intercept extrapolated to $V_{eff} = 0$ V provides an experimental determination of Φ_{B0}, while the slope corresponds to α. By following the aforementioned methodology we can obtain clear signature plots that allow the deciphering of the transport mechanism and provide quantitative measures of interfaces in metal-TiO_2-metal structures. Moreover, this analysis does not require an accurate knowledge of the Richardson constant for the amorphous MO as this might differ by orders of magnitude with respect to its commonly adopted value for silicon. This further highlights the necessity for implementing a temperature-dependent characterization.

3.2. The top electrode

The TE/TiO_2 contacts have been assessed to date mainly through evaluating the DUT's resistance at a specific read-out voltage, typically of 1 V. Here we aim to present an approach focusing more on a quantitative extraction of parameters with physical meaning, i.e. the zero bias potential barrier at the interface, Φ_{B0}. To do this, several configurations having different TEs were fabricated on the same wafer, with the TiO_2 active layer films deposited on top of the Au BE during the same process step. Therefore, with the exception of the TE interface, identical characteristics are expected. To the contrary, the results depicted in figure 3 provide evidence that the TE deposition plays a major role in the characteristics of the device. For the *I–V*s, the discrepancy appearing at $V = 0$ V, as earlier mentioned, arises from our data acquisition system. However, *I–V*s not crossing the zero voltage point are also expected in our case, due to the change in the dominant Schottky contact at the point where the bias polarity changes [51]. Moreover, it is worth mentioning, particularly for the metal/electrolyte systems, that this behaviour has also been correlated with the nanobattery effect [30]. A more detailed study of this aspect will require precise measurements around zero.

Using Ti and Al as a TE result in no rectifying barrier formation, and thus core material controlled conductivity, depicted by the symmetric *I–V* curves (figure 3(a)). Despite the identical (by fabrication) core films, differences in conductivity are obtained. A possible mechanism for the role of metal electrodes on the device resistivity is proposed in [39],

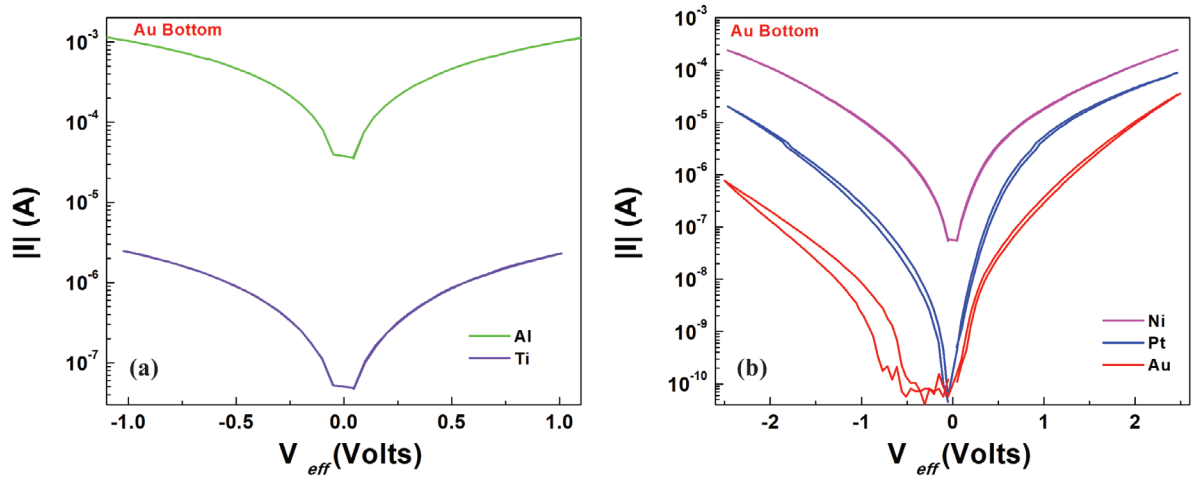

Figure 3. Al and Ti as a TE result in a symmetric *I–V*, denoting no formation of an interface barrier (a). Asymmetric *I–V*s obtained in the cases of Au, Pt and Ni, suggesting an interface-controlled conduction mechanism (b).

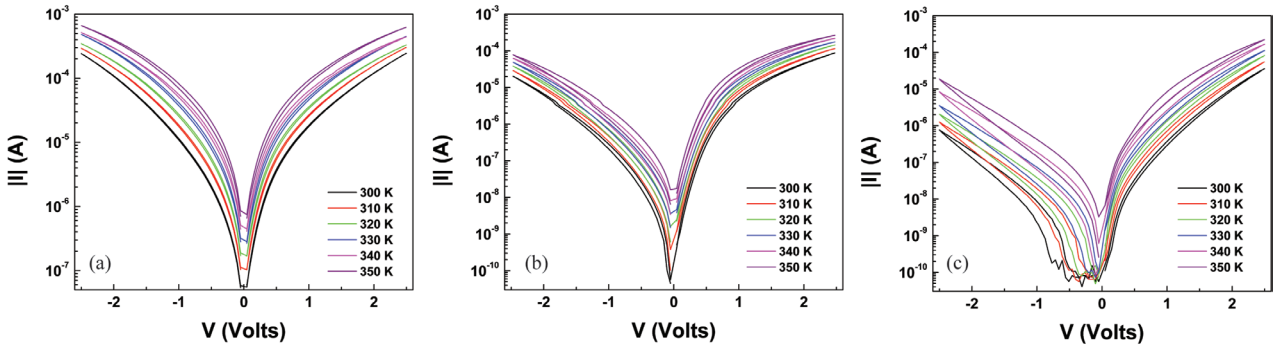

Figure 4. *I–V* curves versus temperature for Ni (a), Pt (b) and Au (c), TE.

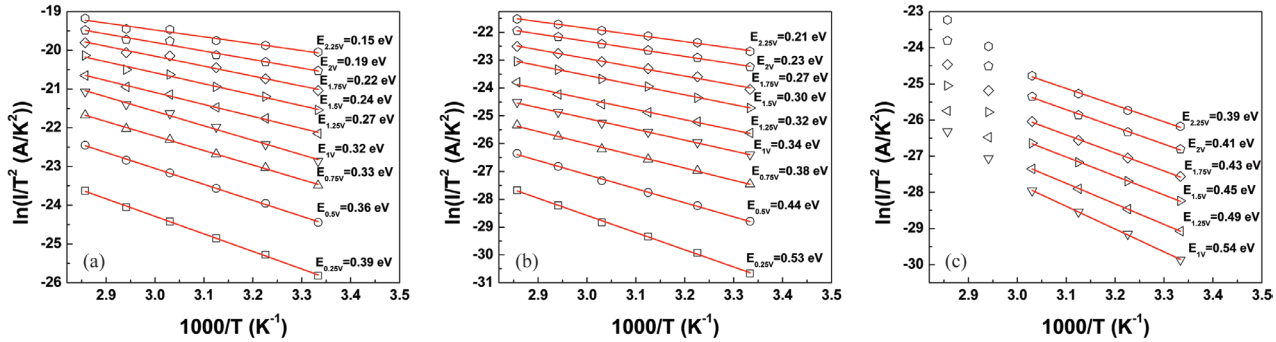

Figure 5. Signature plots (*I–V*s at figure 4) of Ni (a), Pt (b) and Au (c), TE respectively, confirming Schottky emission as the dominant transport mechanism.

based on the Ellingham diagram, where the argument is that electrode metals interact with TiO_2 generating oxygen vacancies. Oxygen vacancies act as n-type dopants, providing free electrons in the MO conduction band and thus determining the device resistance. The relation is not necessary straightforward, however, as in wide band gap materials the conductivity is also determined by the properties of the gap states through mechanisms such as hopping and Poole–Frenkel. Nevertheless, a thorough investigation of the conduction mechanism through the film was not our main intent in this work.

When Au, Pt and Ni (figure 3(b)) are used as the TE, interface barriers are formed, as denoted by the asymmetric *I–V* curves (figure 3(b)). For these materials, a detailed temperature characterization (figure 4) was performed and clear signature plots were extracted (figure 5). This led to the calculation of the zero bias potential barrier Φ_{B0} and the barrier lowering factor α (figure 6(a)) that are summarized in table 1. For these TE materials the conductivity is controlled by thermionic emission over the interface barriers, as confirmed by the clear signature plots (figures 5 and 6(a)).

Considering our pristine (not electroformed) and almost stoichiometric TiO_{2-x} films, a low concentration of mobile ions is expected and the interface barrier should in principle be proportional to the metal work function [46] (W_f [52]). But in cases where a large amount of defect states are present at

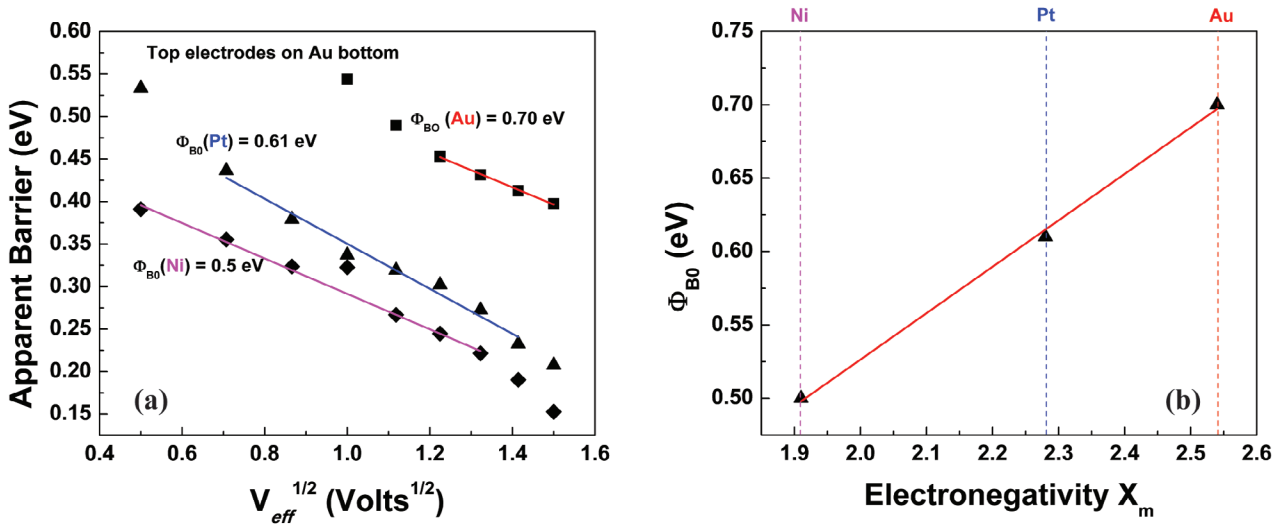

Figure 6. Experimental verification for the conduction mechanism and extraction of the zero bias potential barrier at the top interface (a). The barrier is found to increase linearly with the electronegativity of the TE material (b).

Table 1. Quantitative results extracted from the experimental data regarding the TE/TiO_2interface.

TE material	W_f (eV)	X_m	Interface barrier at TE	Additional information
Al	4.28	1.61	Non-rectifying contact	
Ti	4.1	1.54	Non-rectifying contact	
Pt	5.65	2.28	0.61 eV	$\alpha = 0.265\,\mathrm{eV}^{1/2}$
Ni	5.15	1.91	0.50 eV	$\alpha = 0.208\,\mathrm{eV}^{1/2}$
Au	5.1	2.54	0.70 eV	$\alpha = 0.203\,\mathrm{eV}^{1/2}$

the interface, the total trapped charge also has an important role [46]. Fermi level pinning resulting in barrier heights independent of or weakly dependent on the metal work function are commonly obtained, as for example in the case of III–V materials [53]. This does not apply to our work, as although the barrier formed is not proportional to the metal work function, significant variations exist for distinct electrode materials. In order to better understand the formation of the interfacial barrier we also have to bear in mind that intermediate thin oxide layers of a few nanometres may be formed at metal/oxide interfaces [37], especially on samples exposed to environmental conditions [36]. Further to this, electrode/electrolyte interfaces may be degraded due to electrode reactions [34], while some induction of oxygen vacancies, acting as equivalent to doping, is also expected [38]. These processes result in the formation of an effective barrier with a height that deviates from the expected theoretical predictions. For ionic materials, the formed barriers have been correlated to the metal electronegativity [46] (X_m [54]). The strength of the correlation is typically assessed by the index S:

$$S = \frac{d\Phi_{B0}}{dX_m}. \tag{6}$$

There is considered to be a strong correlation to electronegativity when the S index approaches 1. For example, for silicon $S = 0.05$, while for SiO_2, $S = 1$ [46]. A clear linear relation is supported by our results depicted in figure 6(b). The calculated index is $S = 0.32$. A similar trend, extracted in a completely different way, is presented in [38] that resulted in $S = 0.55$, including materials such as Al and Ti, which in our case appear not to form an interface barrier. This is referred to as partial Fermi pinning that showcases the important role of interface states.

At this point it is worth noting an issue that has not been pointed out to date. This is the obtained inter-relationship between the two interfaces. Throughout this study, we employ this term to highlight that the TE material also results in modifications to the BE interfaces (positive biases in the *I–V*). Considering that the BE and the TiO_2 should be identical, due to common fabrication, we consider this an interesting finding and therefore it is discussed in more detail in the following section.

3.3. Top/bottom electrode inter-relationship

The TE material is found to affect the bottom Au/TiO_2 contacts (figure 3, positive biases) that are nominally identical for all employed prototype devices. In the cases of Al and Ti, no barrier is formed and therefore the conductivity is mainly determined by the film properties. In contrast, depositing Ni, Pt or Au as the TE appears also to instigate the formation of a barrier at the bottom interface, offering the opportunity to perform a quantitative study regarding the role of the TE to the BE interface.

Before proceeding to this analysis, however, it is essential to confirm that the differences obtained in the postitive part of the *I–V*s are not the effect of the forward biased TE Schottky contact. For this we initially assumed that the BE is indeed ohmic, and the current flow is then described by equation (3), resulting in a forward biased Schottky contact. In this case, by differentiating (and for $V > 3$ KT q^{-1}), we obtain

$$\frac{dV}{d(LnI)} = RI + n\frac{\mathrm{KT}}{\mathrm{q}}. \tag{7}$$

Therefore, a plot of $dV/d(LnI)$ versus I should give a straight line with a slope corresponding to series resistance R and the intercept

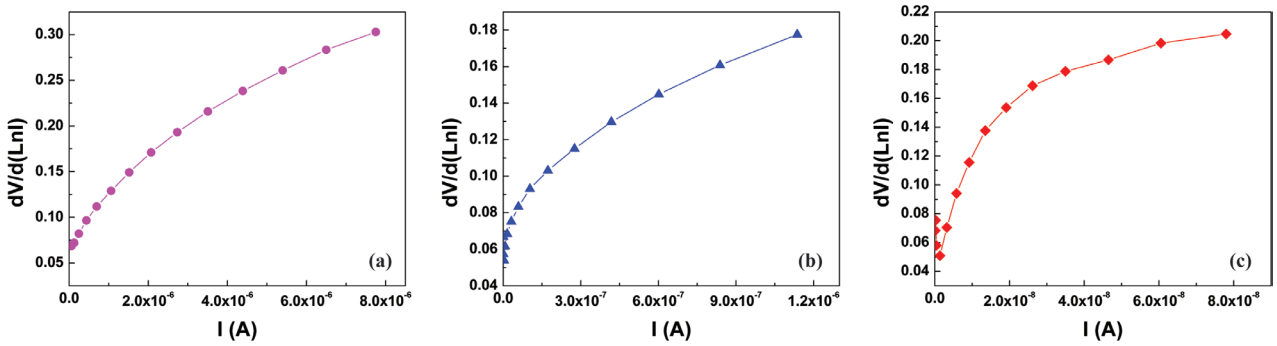

Figure 7. *dV*/*d*(*LnI*) plots for (a) Ni, (b) Pt and (c) Au TEs. In the case of an ohmic bottom contact, a straight line is expected, which is clearly not the case for any of the TE materials used.

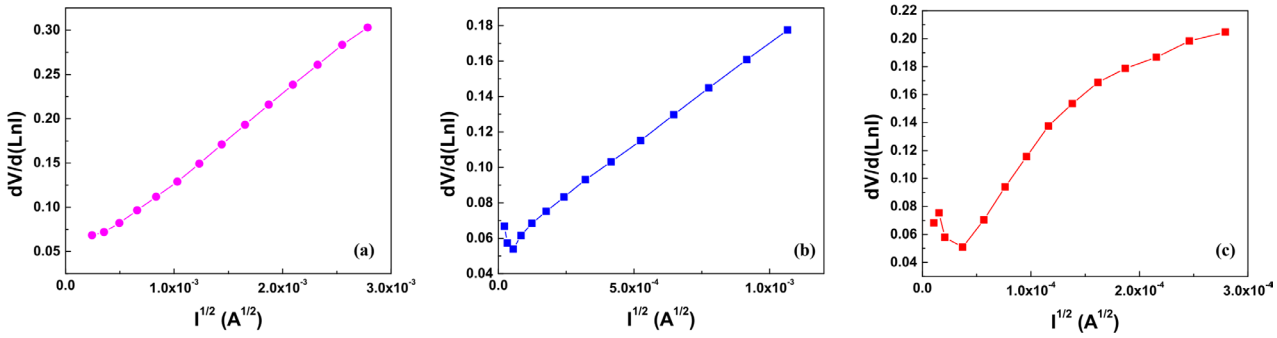

Figure 8. *dV*/*d*(*LnI*) plots for (a) Ni, (b) Pt and (c) Au TEs, as modified for variable series resistance due to SCLC (equation (10)).

to the ideality factor n [55]. The plots for Ni, Pt and Au TEs are shown in figure 7 where clearly no linearity was observed.

Another potential conduction mechanism, in the case of an ohmic BE, is space charge limited currents (SCLCs). SCLCs are commonly obtained in wide band gap materials and insulators when electrons are injected from the electrodes and no compensation charge exists. Typically, SCLCs present an ohmic dependence for low biases, followed by a regime where the traps dominate the process and $I \sim V^m$ with $m > 2$ [56]. For higher biases and injection conditions, the SCLC density J is given by equation (8) [46]:

$$J = \frac{8}{9}\epsilon\mu\frac{V^2}{d^3} \tag{8}$$

where ε is the dielectric permittivity, μ the electron mobility and d the film thickness.

In this case, where the series resistance is not constant, we can then write from equation (8):

$$R\,(I) = \frac{V}{I} \sim I^{-1/2}. \tag{9}$$

By subtracting R in equation (3) with equation (9) and by differentiating, equation (7) modifies to equation (10):

$$\frac{dV}{d(LnI)} = \text{const}^* I^{1/2} + n\frac{\text{KT}}{\text{q}}. \tag{10}$$

Thus a linear relation in a plot of $dV/d(LnI)$ versus $I^{1/2}$ is expected. The results for the TE metals are presented in figure 8.

In addition to this, for high biases where any interface barrier (forward or reverse biased, equation (4)) is diminished, the SCLC should obey equation (8) by showing V^2 dependence and very weak (or negligible, for a narrow temperature range) temperature variation possibly due to changes in the electron mobility.

Table 2. Quantitative results extracted from the experimental data regarding the bottom interface with respect to the TE materials.

TE material	W_f (eV)	X_m	Interface barrier at BE	Additional information
Al	4.28	1.61	Non-rectifying contact	
Ti	4.1	1.54	Non-rectifying contact	
Pt	5.65	2.28	0.54 eV	$\alpha = 0.279\,\text{eV}^{1/2}$
Ni	5.15	1.91	0.37 eV	$\alpha = 0.161\,\text{eV}^{1/2}$
Au	5.1	2.54	0.67 eV	$\alpha = 0.236\,\text{eV}^{1/2}$

Although the results presented in figure 8 may be considered as supportive to equation (10) in the case of Pt (figure 8(b)) (fitting the linear regimes for Ni (figure 8(a)) and Au (figure 8(c)) TE results in ideality factor $n < 1$), the current–voltage dependence does not obey equation (8) as presented in figure 9, while a strong temperature effect is also presented in figure 4. Such a bias dependence ($m > 2$) obtained above $V = 2$ V along with the temperature variation may be attributed to traps-controlled SCLC. This indicates that the devices have not reached the high injection regime (equation (8)), and thus for lower biases ($V < 2$ V) an ohmic dependence is expected rather than the one indicated by equation (8). However, the latter is supported neither by figure 7 (equation (7)) nor by figure 9.

Considering all these aspects, the Au(BE)/TiO_2 interfaces have been further assessed in detail following the previously employed temperature-dependent methodology. The obtained

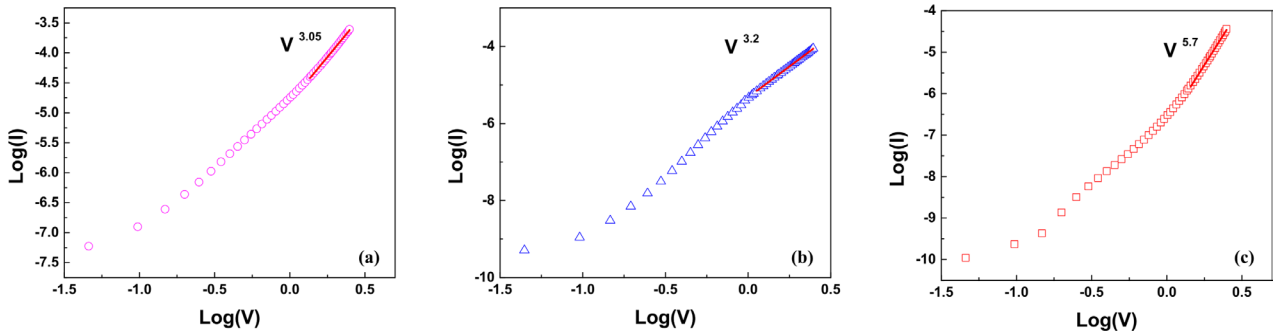

Figure 9. Log–log plots for (a) Ni, (b) Pt and (c) Au TEs, showing potential SCLC signature.

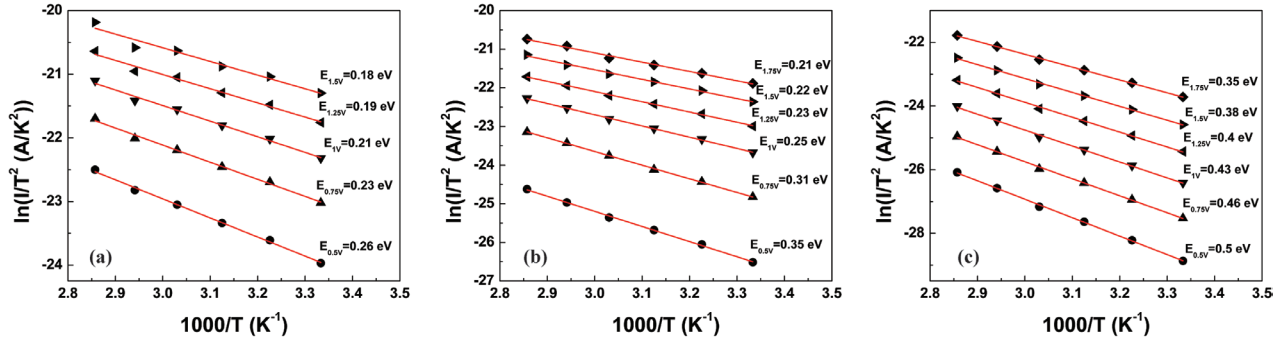

Figure 10. Signature plots (*I–Vs* at figure 4) correspond to the bottom interface, for Ni (a), Pt (b) and Au (c) TEs, confirming Schottky emission as the dominant transport mechanism.

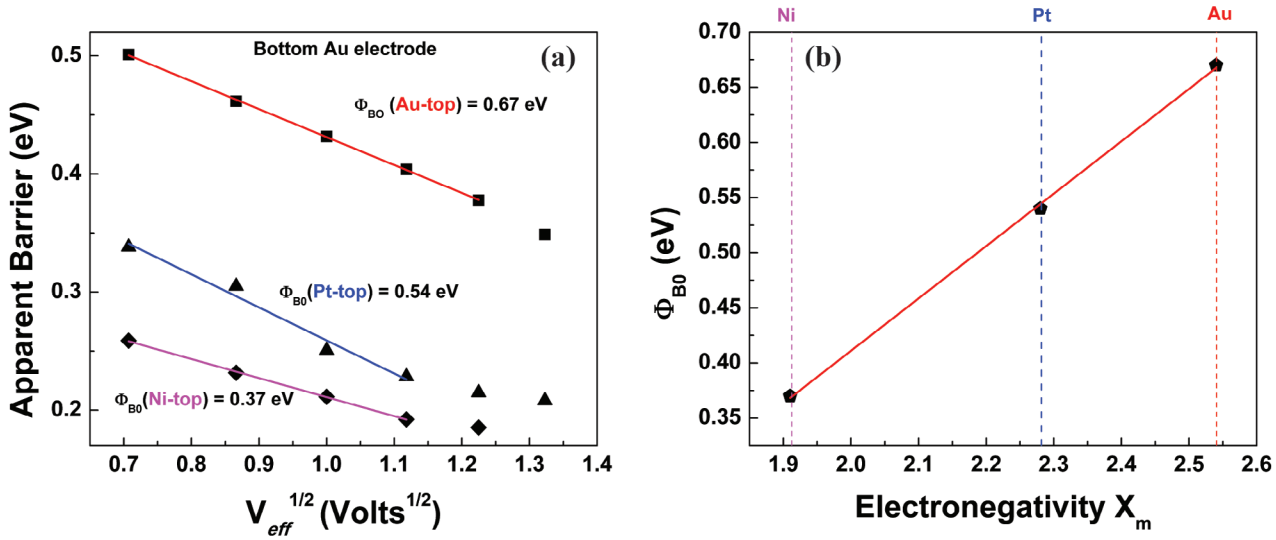

Figure 11. Further experimental verification for the conduction mechanism and extraction of the zero bias potential barrier at the interface for the bottom interface (a). The barrier is found to increase linearly with the electronegativity of the TE material (b).

results for the Au/TiO_2 BE with respect to the TE material are summarized in table 2, while the corresponding signature plots are presented in figure 10. The fitting results (signatures) strongly support this analysis. A linear relation to the electronegativity of the TE material was also obtained for the BE interface barriers. In this case, the barriers formed are lower than those for the TEs but the same trend is followed. The data presented in figure 11 lead to $S = 0.48$. This clearly depicts the influence of the TE material throughout the TiO_2 all the way to the BE, but also signifies the major role of the interface states.

It is worth noting that while this feature was identified for the TE, it is not the case for the BE, highlighting the differences in the formation mechanisms of the two interfaces.

3.4. The bottom electrode

It is quite possible for the BE–TiO_2 interface to show a distinct behaviour to an identical interface, in terms of electrode material, lying at the top of a device, due to processing-induced effects. The up-to-date published works have typically used non-rectifying junctions for the BE, solely targeting the

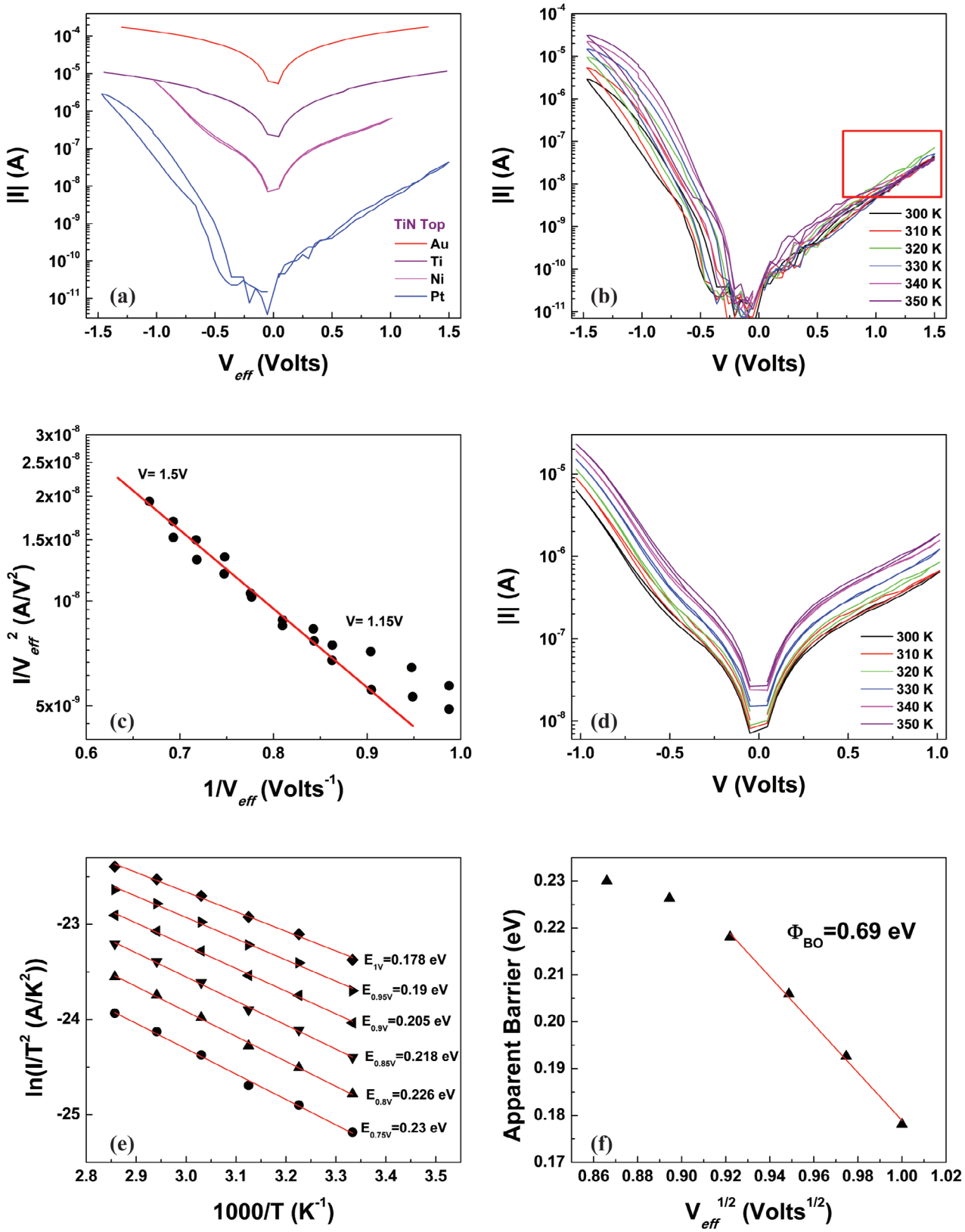

Figure 12. Devices having identical TiN TEs and different BEs were assessed (a). Tunnelling was identified in the case of Pt BE signature plots ((b) and (c)) and Schottky emission when Ni is the BE ((d), (e) and (f)).

influence on the top interface characteristics and assuming similar signatures for both interfaces due to symmetry. Nonetheless, we recently demonstrated that even symmetric structures may overall render an asymmetric performance [57].

The *I–V* characteristics of structures having Au, Ti, Ni and Pt as the BE are presented in figure 12(a). The study was performed on a separate wafer target fabricated for this study (figure 1(b)). In all cases the TE is TiN deposited by

Table 3. Results extracted from the experimental data regarding the BE materials.

BE material	W_f (eV)	X_m	Interface barrier	Additional information
Au	5.1	2.54	Non-rectifying contact	
Ti	4.1	1.54	Non-rectifying contact	
Ni	5.15	1.91	0.69 eV	$\alpha = 0.511\,\mathrm{eV}^{1/2}$
Pt	5.65	2.28	Very high	Tunnelling

sputtering. By observation of the acquired symmetric *I–V*s, it follows that no interface barrier is formed in the cases where Au and Ti were used as BEs, denoting that the overall conductivity is controlled by the TiO_2 thin-film. Besides, the two structures exhibit different conductivities, suggesting that the BE material also plays a major role on the electrical properties of the deposited film. In cases where Pt and Ni were used as the BE, strongly asymmetric *I–V* characteristics were obtained, denoting an interface-controlled transport. In these cases, the *I–V* characteristics have been further assessed in the temperature range of 300 K–350 K in order to obtain the corresponding signature plots. The applied biases have been limited to 1.5 V and 1 V respectively, so as to avoid the devices undergoing either a soft or irreversible (hard) breakdown. For the sample with a Pt BE (figure 12(b)), the part of *I–V* plot corresponding to the BE (positive biases) presents a temperature-independent behaviour (highlighted in the red square). This, along with the signature plot presented in figure 12(c), supports the conclusion that tunnelling is the major mechanism responsible for the conductivity, indicating the presence of quite a high barrier at this interface, but which cannot be measured via equation (2).

Conversely, for the device formed atop the Ni BE (figure 12(d)), signature plots have been obtained that confirm thermionic emission over the interface barrier as the dominant transport mechanism. The data analysis led to the estimation of the zero bias potential barrier at the interface (figures 12(e) and (f)). The results for the BE study are summarized in table 3 along with the metal work function and electronegativity, as those parameters may determine the interface barrier.

The differences obtained when the same metals were used as TE or BE could be assigned both to differences in the two interfaces as well as the core area of the film. It has been reported that BE materials may affect the concentration of the ions in the film [58], while local imperfections, e.g. roughness, could play a major role on the film microstructures [59], and thus both parameters can in turn modify the electrical response of the device. These two parameters are also heavily involved in the formation of the interface barrier. However, this is a much more complicated issue. The BE is the first layer that is deposited and thus this interface is more exposed during the sequential fabrication steps and the environmental influences than the top one, which is typically the last step before the characterization [58]. Moreover, during the oxide film deposition highly energetic particles are coming into contact with the BE material, making the local formation of the interfacial layer sensitive to this process step [34]. Conversely, for the upper layers of the film, the new deposited particles are hosted on a well-formed oxide film, rendering the formation of the top interface completely different to that of the BE. Therefore, identical metals form quite different barriers when used as TEs or BEs [57]. We note, however, that no straightforward quantitative correlation can be obtained at this stage for the BE, nor for its influence on the top interface. Therefore our results should raise attention to the necessity for more thorough and targeted studies towards understanding and control of the BE/TiO_2 interface. Ni as a BE results in Schottky behaviour for the TiN TE, whilst in the case of Pt, the important hysteresis presented in figure 10(b) denotes the notable contribution of ions that do not allow for the accurate extraction of parameters for the TiN TE (in the presence of a sufficient number of mobile ions, the conventional Schottky analysis is not valid), although its rectifying character is revealed.

3.5. Discussion

This study has provided several new insights into the electrical properties of metal-TiO_2 interfaces. Evidently, these cannot be considered as conventional metal–semiconductor contacts, where the formation of the interface barrier is determined by the metal work function. Our quantitative results suggest that there are many parameters involved in the formation of these barriers, not in a straightforward manner, and therefore the drawing of concluding remarks should be based on carefully selected experimental comparisons and observations. Considering these, and for the devices fabricated on the same wafer having nominally identical Au BE and TiO_2 active layers deposited during the same process, we can reliably demonstrate the following.

Regarding the top contacts, two major regimes obtained. Al and Ti TEs do not form a rectifying barrier. In these cases the conductivity of the structure is determined by the TiO_2 film. This is found to be affected by the TE material, possibly due to interactions leading to an increase in oxygen vacancies. Conversely, in the cases of Ni, Pt and Au TEs, an interface barrier is formed and we can present some clear conclusions. The barrier height at the top interface is found to be proportional to the metal electrode electronegativity, highlighting the important role of the interface reactions in the formation of these barriers. The proportionality factor (*S* index) is far from 1, thus denoting the major contribution of the interface states (partial pinning). This study also came across an unexpected observation (interface inter-relationship), where the common Au BE interface barrier is not identical but was found to be determined by the TE material. Non-rectifying and electronegativity dependent barriers obtained, respectively. This requires that the metal electrodes are selected in pairs, as the TE defines the properties of the bottom interface as well. Considering this interesting finding, which has not been reported before, a thickness dependence study will be a natural progression to further verify our results. Therefore, comparisons performed on different stacks should be carefully considered as they may lead to serious misinterpretations.

Regarding the BE, the same trend does not apply, i.e. the BE barrier is not determined by the electronegativity. It is therefore concluded that different mechanisms are responsible for the formation of the interfaces in the BE cases, where the TiO_2 film is deposited on the metal, in contrast to the TE interfaces where the metal is deposited atop the TiO_2 film. This is consistent with our previous study, where an asymmetric barrier obtained on purely symmetric contacts [57]. However, the BE also seems to affect the top interfaces, as presented by our results on devices having identical films and TiN TEs, but not with a straightforward quantitative relationship, however. This further supports our argument that electrode materials should always be selected in pairs. Moreover, each material should be carefully considered with respect to its use as a TE or BE; although in some cases, such as Ti, no rectifying barrier is formed for either configuration, rendering the Ti/TiO_2/Ti system as the most suitable with which to study the film-controlled transport [50].

Considering the growth of and the prospects [15, 16] for oxide-based applications, including the Internet of Things, wearable electronics, reconfigurable and/or bio-inspired systems, the major role of TiO_2-based electronic devices, as well as the necessity for metal electrodes on top of or below their active area, we proceed by sharing some thoughts on the usefulness of our results across diverse MO applications. In the field of RRAM, where typically the devices are used after an electroforming step, Schottky barriers are considered essential for supporting resistive switching [60]. It was also reported that high barriers support both unipolar and bipolar resistive switching, in contrast to lower barriers that typically favour bipolar operation [61]. Moreover, metal-oxide interfaces are critical in determining the operation of both valence change memories (VCMs) and electrochemical metallization cells through the formation of barriers and electrochemical reactions [34]. The proper selection of metal electrodes can be used to engineer the electroforming process, in terms of polarity and applied field intensity, and perhaps even in developing forming-free RRAM technologies. The electrodes' characteristics are also of major importance to semiconductor devices. For example, when considering TiO_2-based bipolar devices it is essential to avoid any rectification stemming from the metal electrodes. Moreover, in the case of TFTs, different configurations may require source and drain electrodes atop or below the deposited MO films defining the TFTs' active area, and thus should be selected accordingly. Finally, several applications require the monolithic integration of such technologies. A prominent example is the use of diodes or transistors as selecting elements [62] for RRAM, rendering 1D1R and/or 1T1R configurations. Such cases typically exploit common metal electrodes acting both as BE and TE for different devices and thus should be accordingly considered, also bearing in mind the TE and BE inter-relationship issues.

4. Conclusions

A quantitative electrical characterization study is presented of the interfacial barriers at metal-TiO_2 contacts. This involved targeted fabrication of metal-TiO_2-metal prototypes, recording of the *I–V* curves at varying temperatures, and analysis through appropriate modelling. Distinct characteristics were identified for contacts formed atop and below the active area films. For Ni, Pt and Au, which form rectifying contacts at the top interface, the barriers were found to be proportional to their electronegativity, showing partial pinning. For those devices the top metal electronegativity also appeared to determine the nominally identical Au/TiO_2 bottom interfaces in a similar manner. For the BE, however, the same trend is not obvious. Despite that, the different BEs were also found to affect the nominally identical top interfaces, but in this case a quantitative correlation is presently not straightforward, suggesting the need for more targeted studies. Overall we may conclude that the electrode materials in TiO_2 devices should be selected in pairs, bearing in mind always their position with respect to the active film (on top or below) and the metal electronegativity in particular for the top ones. Our results act as a very useful background for the wide range of TiO_2-based applications covering RRAMs, TFTs, bipolar semiconductor devices and monolithic integration, including 1T1R structures.

Acknowledgments

This work was supported by EPSRC Grants EP/R024642/1 and EP/K017829/1.

Data availability

All data supporting this study are openly available from the University of Southampton repository at: https://doi.org/10.5258/SOTON/D0630.

ORCID iDs

L Michalas https://orcid.org/0000-0002-0753-2574
S Stathopoulos https://orcid.org/0000-0002-0833-6209
T Prodromakis https://orcid.org/0000-0002-6267-6909

References

[1] Yu X, Marks T J and Facchetti A 2016 Metal oxides for optoelectronic applications *Nat. Mater.* **15** 383–96
[2] Brox-Nilsen C, Jidong J, Yi L, Peng B and Song A M 2013 Sputtered ZnO thin-film transistors with carrier mobility over 50 $cm^2 V^{-1} s^{-1}$ *IEEE Trans. Electron Devices* **60** 3424–9
[3] Kim W, Chattopadhyay A, Siemon A, Linn E, Waser R and Rana V 2016 Multistate memristive tantalum oxide devices for ternary arithmetic *Sci. Rep.* **6** 36652
[4] Stathopoulos S, Khiat A, Trapatseli M, Cortese S, Serb A, Valov I and Prodromakis T 2017 Multibit memory operation of metal-oxide bi-layer memristors *Sci. Rep.* **7** 17532
[5] Ielmini D 2016 Resistive switching memories based on metal oxides: mechanisms, reliability and scaling *Semicond. Sci. Technol.* **31** 063002
[6] Sawa A 2008 Resistive switching in transition metal oxides *Mater. Today* **11** 28–36

[7] Park J S, Maeng W J, Kim H S and Park J S 2012 Review of recent developments in amorphous oxide semiconductor thin-film transistor devices *Thin Solid Films* **520** 1679–93

[8] Kamiya T, Nomura K and Hosono H 2009 Origins of high mobility and low operation voltage of amorphous oxide TFTs: electronic structure, electron transport, defects and doping *J. Disp. Technol.* **5** 273–88

[9] Rühle S, Anderson A Y, Barad H N, Kupfer B, Bouhadana Y, Rosh-Hodesh E and Zaban A 2012 All-oxide photovoltaics *J. Phys. Chem. Lett.* **3** 3755–64

[10] Fine G F, Cavanagh L M, Afonja A and Binions R 2010 Metal oxide semi-conductor gas sensors in environmental monitoring *Sensors* **10** 5469–502

[11] Petti L, Münzenrieder N, Vogt C, Faber H, Büthe L, Cantarella G, Bottacchi F, Anthopoulos T D and Tröster G 2016 Metal oxide semiconductor thin-film transistors for flexible electronics *Appl. Phys. Rev.* **3** 021303

[12] Liu Y, Pharr M and Salvatore G A 2017 A lab-on-skin: a review of flexible and stretchable electronics for wearable health monitoring *ACS Nano* **11** 9614–35

[13] Serb A, Bill J, Khiat A, Berdan R, Legenstein R and Prodromakis T 2016 Unsupervised learning in probabilistic neural networks with multi-state metal-oxide memristive synapses *Nat. Commun.* **7** 12611

[14] Mehonic A and Kenyon A J 2016 Emulating the electrical activity of the neuron using a silicon oxide RRAM cell *Frontiers Neurosci.* **10** 57

[15] Myny K 2018 The development of flexible integrated circuits based on thin-film transistors *Nat. Electron.* **1** 30–9

[16] Zidan M A, Strachan J P and Lu W D 2018 The future of electronics based on memristive systems *Nat. Electron.* **1** 22–9

[17] Strukov D B, Snider G S, Stewart D R and Williams R S 2009 The missing memristor found *Nature* **459** 1154

[18] Shih W S, Young S J, Ji L W, Water W and Shiu H W 2011 TiO_2-based thin film transistors with amorphous and anatase channel layer *J. Electrochem. Soc.* **158** H609–11

[19] Choi H, Shin J and Shin C 2017 Impact of source/drain metal work function on the electrical characteristics of anatase TiO_2-based thin film transistors *ECS J. Solid State Sci. Technol.* **6** 379–82

[20] Bai J and Zhou B 2014 Titanium dioxide nanomaterials for sensor applications *Chem. Rev.* **114** 10131–76

[21] Trapatseli M, Khiat A, Cortese S, Serb A, Carta D and Prodromakis T 2016 Engineering the switching dynamics of TiO_x-based RRAM with Al doping *J. Appl. Phys.* **120** 025108

[22] Zhao L, Park S G, Magyari-Köpe B and Nishi Y 2013 Dopant selection rules for desired electronic structure and vacancy formation characteristics of TiO_2 resistive memory *Appl. Phys. Lett.* **102** 083506

[23] Anitha V C, Banerjee A N and Joo S W 2015 Recent developments in TiO_2 as n- and p-type transparent semiconductors: synthesis, modification, properties, and energy-related applications *J. Mater. Sci.* **50** 7495–536

[24] Wang Z, Nayak P K, Caraveo-Frescas J A and Alshareef H N 2016 Recent developments in p-type oxide semiconductor materials and devices *Adv. Mater.* **28** 3831–92

[25] Hazra A, Chattopadhyay P P and Bhattacharyya P 2015 Hybrid fabrication of highly rectifying p–n homojunction based on nanostructured TiO_2 *IEEE Electron Device Lett.* **36** 505–7

[26] Vasu K, Sreedhara M B, Ghatak J and Rao C N R 2016 Atomic layer deposition of p-type epitaxial thin films of undoped and N-doped anatase TiO_2 *ACS Appl. Mater. Interfaces* **8** 7897–901

[27] Hossein-Babaei F, Gharesi M and Moalaghi M 2017 Diffusion bonding of metal wires directly to the functional metal oxide semiconductors for forming reliable electrical contacts *ACS Appl. Mater. Interfaces* **9** 26637–41

[28] Hossein-Babaei F, Moghadam S and Masoumi S 2015 Forming ohmic Ag/SnO_2contacts *Mater. Lett.* **141** 141–4

[29] Ashworth D G, Oven R and Page M C 2017 Field-assisted diffusion of silver in SnO_2 thin films *J. Phys. Conf. Ser.* **939** 012007

[30] Valov I, Linn E, Tappertzhofen S, Schmelzer S, Van Den Hurk J, Lentz F and Waser R 2013 Nanobatteries in redox-based resistive switches require extension of memristor theory *Nat. Commun.* **4** 1771–9

[31] Tappertzhofen S, Waser R and Valov I 2014 Impact of the counter-electrode material on redox processes in resistive switching memories *ChemElectroChem* **1** 1287–92

[32] Lubben M, Karakolis P, Ioannou-Sougleridis V, Normand P, Dimitrakis P and Valov I 2015 Graphene-modified interface controls transition from VCM to ECM switching modes in Ta/TaO_x based memristive devices *Adv. Mater.* **27** 6202–7

[33] Tappertzhofen S, Valov I, Tsuruoka T, Hasegawa T, Waser R and Aono M 2013 Generic relevance of counter charges for cation-based nanoscale resistive switching memories *ACS Nano* **7** 6396–402

[34] Valov I 2017 Interfacial interactions and their impact on redox-based resistive switching memories (ReRAMs) *Semicond. Sci. Technol.* **32** 093006

[35] Hossein-Babaei F and Navid Alae-Sheini M M L 2016 Oxygen adsorption at noble metal/TiO_2 junctions *IOP Conf. Ser.: Mater. Sci. Eng.* **108** 012030

[36] Lübben M, Wiefels S, Waser R and Valov I 2018 Processes and effects of oxygen and moisture in resistively switching TaO_x and HfO_x *Adv. Electron. Mater.* **4** 1700458

[37] Cho D Y, Luebben M, Wiefels S, Lee K S and Valov I 2017 Interfacial metal-oxide interactions in resistive switching memories *ACS Appl. Mater. Interfaces* **9** 19287–95

[38] Zhong N, Shima H and Akinaga H 2010 Rectifying characteristic of Pt/TiO_x/metal/Pt controlled by electronegativity *Appl. Phys. Lett.* **96** 042107

[39] Yang J J, Strachan J P, Miao F, Zhang M X, Pickett M D, Yi W, Ohlberg D A A, Medeiros-Ribeiro G and Williams R S 2011 Metal/TiO_2 interfaces for memristive switches *Appl. Phys.* A **102** 785–9

[40] Hossein-Babaei F, Lajvardi M M and Alaei-Sheini N 2015 The energy barrier at noble metal/TiO_2 junctions *Appl. Phys. Lett.* **106** 083503

[41] Serb A, Khiat A and Prodromakis T 2018 Seamlessly fused digital-analogue reconfigurable computing using memristors *Nat. Commun.* **9** 2170

[42] Carta D, Mountjoy G, Regoutz A, Khiat A, Serb A and Prodromakis T 2015 X-ray absorption spectroscopy study of TiO_{2-x} thin films for memory applications *J. Phys. Chem.* C **119** 4362–70

[43] Berdan R, Serb A, Khiat A, Regoutz A, Papavassiliou C and Prodromakis T 2015 A μ-controller-based system for interfacing selectorless RRAM crossbar arrays *IEEE Trans. Electron Devices* **62** 2190–6

[44] Tsuruoka T, Terabe K, Hasegawa T, Valov I, Waser R and Aono M 2012 Effects of moisture on the switching characteristics of oxide-based, gapless-type atomic switches *Adv. Funct. Mater.* **22** 70–7

[45] Michalas L, Koutsoureli M, Saada S, Mer-Calfati C, Leuliet A, Martins P, Bansropun S, Papaioannou G, Bergonzo P and Ziaei A 2014 Electrical assessment of diamond MIM capacitors and modeling of MEMS capacitive switch discharging *J. Micromech. Microeng.* **24** 115017

[46] Sze S M and Ng K K 2007 *Physics of Semiconductor Devices* (New York: Wiley)

[47] Schaub R, Wahlstro E, Rønnau A, Lægsgaard E, Stensgaard I and Besenbacher F 2006 Oxygen-mediated diffusion of TiO_2 (1 1 0) surface *Science* **299** 377–9

[48] Wedig A *et al* 2016 Nanoscale cation motion in TaO_x, HfO_x and TiO_xmemristive systems *Nat. Nanotechnol.* **11** 67–74

[49] Hossein-Babaei F and Alaei-Sheini N 2017 A model for the electric conduction in metal/poly-TiO_2metal structure *J. Phys.: Conf. Ser.* **939** 012010
[50] Hossein-Babaei F and Alaei-Sheini N 2016 Electronic conduction in Ti/Poly-TiO_2/Ti structures *Sci. Rep.* **6** 29624
[51] Fu J *et al* 2016 Stability and its mechanism in Ag/CoO_x/Ag interface-type resistive switching device *Sci. Rep.* **6** 35630
[52] www.kayelaby.npl.co.uk/atomic_and_nuclear_physics/4_3/4_3.html
[53] Hasegawa H 1999 Fermi level pinning and Schottky barrier height control at metal-semiconductor interfaces of InP and related materials *Japan. J. Appl. Phys.* **38** 1098–102
[54] Allred A L 1961 Electronegativity values from thermochemical data *J. Inorg. Nucl. Chem.* **17** 215–21
[55] Cheung S K and Cheung N W 1986 Extraction of Schottky diode parameters from forward current-voltage characteristics *Appl. Phys. Lett.* **49** 85–7
[56] Lampert M A 1956 Simplified theory of space-charge-limited currents in an insulator with traps *Phys. Rev.* **103** 1648–56
[57] Michalas L, Trapatseli M, Stathopoulos S, Cortese S, Khiat A and Prodromakis T 2017 Interface asymmetry induced by symmetric electrodes on metal-Al:TiOx-metal structures *IEEE Trans. Nanotechnol.* **17** 867–72
[58] Lübben M, Menzel S, Park S G, Yang M, Waser R and Valov I 2017 SET kinetics of electrochemical metallization cells: influence of counter-electrodes in SiO_2/Ag based systems *Nanotechnology* **28** 135205
[59] Munde M S, Mehonic A, Ng W H, Buckwell M, Montesi L, Bosman M, Shluger A L and Kenyon A J 2017 Intrinsic resistance switching in amorphous silicon suboxides: the role of columnar microstructure *Sci. Rep.* **7** 9274
[60] Hernández-Rodríguez E, Márquez-Herrera A, Zaleta-Alejandre E, Meléndez-Lira M, La Cruz W D and Zapata-Torres M 2013 Effect of electrode type in the resistive switching behaviour of TiO_2 thin films *J. Phys. D.: Appl. Phys.* **46** 045103
[61] Kim W-G and Rhee S-W 2010 Effect of the top electrode material on the resistive switching of TiO_2 thin film *Microelectron. Eng.* **87** 98–103
[62] Cortese S, Khiat A, Carta D, Light M E and Prodromakis T 2016 An amorphous titanium dioxide metal insulator metal selector device for resistive random access memory crossbar arrays with tunable voltage margin *Appl. Phys. Lett.* **108** 033505